Automatika

Journal for Control, Measurement, Electronics, Computing and Communications

ISSN: 0005-1144 (Print) 1848-3380 (Online) Journal homepage: https://www.tandfonline.com/loi/taut20

Robust adaptive neural network control for switched reluctance motor drives

Cunhe Li, Guofeng Wang, Yan Li & Aide Xu

To cite this article: Cunhe Li, Guofeng Wang, Yan Li & Aide Xu (2018) Robust adaptive neural network control for switched reluctance motor drives, Automatika, 59:1, 24-34, DOI: 10.1080/00051144.2018.1486797

To link to this article: https://doi.org/10.1080/00051144.2018.1486797

AUTOMATIKA
2018, VOL. 59, NO. 1, 24–34
https://doi.org/10.1080/00051144.2018.1486797

REGULAR PAPER

OPEN ACCESS Check for updates

Robust adaptive neural network control for switched reluctance motor drives

Cunhe Li, Guofeng Wang, Yan Li and Aide Xu

Shool of Information Science and Technology, Dalian Maritime University, Dalian, People's Republic of China

ABSTRACT

This article presents a robust adaptive neural network controller for switched reluctance motor (SRM) speed control with both parameter variations and external load disturbances. The radial basis function neural network with the technology of minimal learning parameters is employed to approximate an ideal control law which includes the parameter variations and external disturbances. Furthermore, a proportional control term is introduced to improve the transient performance and chattering phenomena of the SRM drive system. The asymptotic stability of the proposed controller is guaranteed through rigorous Lyapunov analysis. A main advantage of the proposed control scheme is that it contains only one adaptive parameter that needs to be updated on-line. This advantage result in a much simpler adaptive control algorithm, which is convenient to implement in switched reluctance drives. Finally, the simulations and experiments are carried out to demonstrate the effectiveness of the proposed control scheme.

ARTICLE HISTORY
Received 29 August 2017
Accepted 1 June 2018

KEYWORDS
Switched reluctance motor; speed control; adaptive neural network control; parameter variations; external load disturbances

1. Introduction

Switched reluctance motor (SRM) drive is a promising competitor of variable speed drive system due to its simple construction, high efficiency and fault tolerance capability. It has been used in many industry applications, including electric vehicle, wind power generation, aviation industry, household appliances and so on [1–3]. However, the severe nonlinearity of electromagnetic torque caused by the double salient structure and discrete commutation from one phase to another makes the speed of SRM difficult to control. Besides, the speed performance of an SRM is quite sensitive to motor parameter variations and external load disturbance. Therefore, many investigations have been undertaken over the past few decades in order to obtain the high quality speed performance of SRM by applying all kinds of control techniques, such as the PID control [4], feedback linearization control [5], internal model control [6], adaptive control [7], variable structure control [8], intelligent control [9–15] and so on.

The intelligent control has the advantage of strong capability of handing uncertain and nonlinear information. Thus, using intelligent algorithm in SRM modelling and control have been extensively studied in the past few years. In [9], a nonlinear model of SRM is established by using the least square and vector machine technique. In [10], the authors develop a back-propagation neural network (NN) to describe the current $i(\psi, \theta)$ and torque $T(\theta, i)$ characteristics. In [11], a two-layer recurrent NN is trained and applied to identify the damper parameters from operating data. But the NN-base control systems require numerous sample data from experiments or finite-element analysis to train the NN off-line, which inevitably takes much time. Moreover, during the motor operation, the NN needs to be stored in processor to guarantee the real-time of control system, which requires a large amount of computational burden for the algorithm execution. This problem can be partially solved by combining the intelligent algorithm and proportional-integral-derivative (PID) control. In [12], a self-tuning fuzzy PID controller which can adaptively adjust controller parameters on-line is developed to regulate the speed of SRM drive system. In [13], based on different fuzzy inference rules, the fuzzy PID controller is designed to solve the position servo control of SRM direct drive volume control hydraulic press. To eliminate the effect of the dead zone of SRM, an improved dead-zone compensation fuzzy logic controller is presented in [14]. However, the expert's control knowledge and operator's experience are always needed to summarize the fuzzy logic rules in these methods. In order to solve this problem, the adaptive technique is incorporated with intelligent algorithms. Based on Lyapunov's stability theory, an adaptive TSK-fuzzy controller with a compensated control is proposed to control the speed of SRM in [15]. In [16], an adaptive fuzzy cerebellar model articulation controller is designed to improve the speed performance of SRM. One main advantage of these schemes is that the parameters of controller were adjusted on-line according to adaptive rules and, therefore, guarantee the robustness of SRM drive system for external load disturbance and motor's parameter variations. Although these control methods have significant

CONTACT Guofeng Wang gfwangsh@163.com Shool of Information Science and Technology, Dalian Maritime University, Dalian, People's Republic of China

advantages, there still exists a weakness that is the number of on-line updated parameters depending on the number of fuzzy rule bases or the number of NN nodes. In order to improve the approximation accuracy, the number of fuzzy rule bases or the number of NN nodes will increased enormously in general. As a result, the on-line learning time will become prohibitively large and then the huge computational burden prohibit the use of this control scheme for practical implementations. Fortunately, this problem was first solved by minimal learning parameters (MLP) technique in [17]. A main feature of this technique is that only one parameter is needed to be estimated on-line. Inspired by the work [17], a new direct adaptive fuzzy control is proposed for nonlinear strict-feedback systems in [18]. However, there is very little work on MLP technique for SRM drive systems.

Therefore, a robust adaptive neural network (RANN) controller is developed to regulate the speed of SRM drive system in this article. A radial basis function (RBF) NN with the MLP technology is employed to approximate the desirable control law of SRM drive system. The parameter variations and external load disturbances of the system are considered to guarantee the robustness of the proposed controller. And the stability of the proposed RANN controller is guaranteed by using rigorous Lyapunov analysis. The key features of the proposed control scheme are that, (1) the number of adaptive parameters that needs to be updated on-line is reduced to one, and (2) the transient performance and chattering phenomena of the system is improved by introducing a proportional control term. These features guarantee that the computational burden of the proposed control scheme is drastically reduced and the proposed control scheme facilitates the implementation in actual SRM drive system. Finally, simulation and experimental results are provided to demonstrate the effectiveness of the proposed control scheme.

The remainder of this article is assigned as follows: the SRM model and problem formulation are presented in Section 2; the RANN controller is designed and then analysis its stability in Section 3; Section 4 presents the numerical simulation results and the experimental results are showed in Section 5; Section 6 contains conclusions.

2. SRM model and problem formulation

In the SRM, only the stator has windings and the rotor consists simply of steel laminations stacked without permanent magnets and conductors. The cross section of a typical three-phases 12/8 poles SRM and its power converter are shown in Figure 1. With the Faraday's law, the pth phase voltage balance equation of the three-phases SRM can be expressed as

$$\frac{\mathrm{d}\psi_p(i_p,\theta)}{\mathrm{d}t} = v_p - R_p i_p, \quad p = 1,2,3, \tag{1}$$

where ψ_p, v_p, R_p, i_p and θ are stator phase flux linkage, stator phase voltage, stator phase resistance, stator phase current and rotor position, respectively.

If we ignore the effect of mutual inductance, the stator flux linkage can be described as

$$\psi_p = L_p(\theta, i_p) \cdot i_p, \tag{2}$$

where $L_p(\theta, i_j)$ is the phase self-inductance.

The most general expression for the electromagnetic torque at any position can be represented as

$$T_e = \left.\frac{\mathrm{d}W_c(\theta,i_p)}{\mathrm{d}\theta}\right|_{i_p=\text{const}} = \left.\frac{\mathrm{d}W_s(\theta,i_p)}{\mathrm{d}\theta}\right|_{\psi_p=\text{const}}, \tag{3}$$

where T_e is the electromagnetic torque, $W_c = \int_0^i \psi(\theta, i)\,\mathrm{d}i$ is the co-energy, $W_s = \int_0^\psi i(\theta,\psi)\,\mathrm{d}\psi$ is the stored field energy. By neglecting the saturation field effects in SRM, the self-inductance L_p becomes independent of the current i_p. In this case, according to (3), the electromagnetic torque T_e can be expressed as

$$T_e = \frac{1}{2}\cdot\frac{\mathrm{d}L_p(\theta)}{\mathrm{d}\theta}\cdot i_p^2 = \frac{1}{2}\cdot\left(\frac{\mathrm{d}L_p(\theta)}{\mathrm{d}\theta} i_p\right) \times \cdot i_p = K_t(\theta, i_p)\cdot i_p, \tag{4}$$

where $K_t(\theta, i_p) > 0$ denotes the torque coefficient.

The electromagnetic dynamic equation of the machine and loads can be expressed as

$$\frac{\mathrm{d}\omega}{\mathrm{d}t} = \frac{1}{J}(T_e - k_\omega\omega - T_L), \tag{5}$$

where J, k_w, and w are the moment of inertia, the viscous frictional and the rotor speed, respectively. T_L is the external load torque.

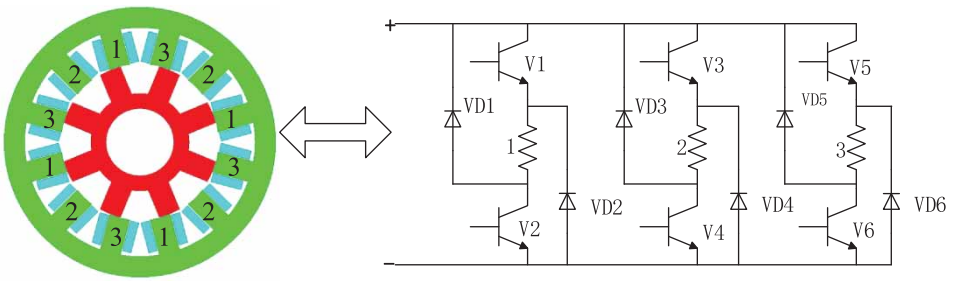

Figure 1. SRM with three-phase asymmetrical half-bridge power converter.

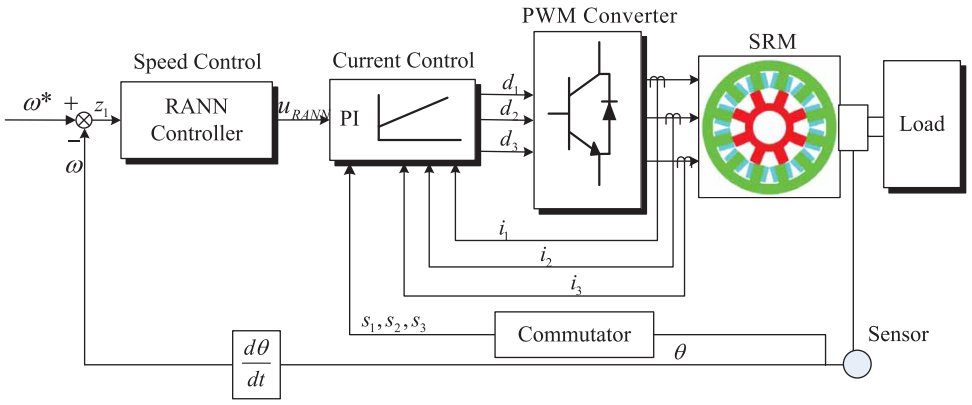

Figure 2. The block diagram of SRM drive system.

2.1. Problem formulation

In practical applications, the SRM operates under different working conditions, which will lead to changes in the parameters of the motor. Hence, the real parameter consists of two parts, the nominal value and their variations. Substituting (4) into (5), we have

$$\begin{aligned}\dot{\omega} &= (A_1 + \Delta A_1)u + (A_2 + \Delta A_2)\omega + (A_3 + \Delta A_3)T_L \\ &= A_1 u + A_2 \omega + \mathrm{d}_L, \end{aligned} \tag{6}$$

where $A_1 = K_t/J$, $A_2 = -k_\omega/J$ and $A_3 = -1/J$ are the nominal values of SRM's parameter. ΔA_1, ΔA_2 and ΔA_3 are variation values of nominal parameters A_1, A_2 and A_3, respectively. d_L denotes the lamped uncertainty of SRM drive system consisting of the parameter variations and external load disturbance.

In this article, the control objective is to design a robust adaptive controller using NN for the speed regulation of SRM drive system with the system uncertainty d_L, so that the motor speed ω can be tracking the speed reference ω^*, while the speed tracking error z_1 tends to zero when the time t tends to infinity. The block diagram of SRM drive system is depicted in Figure 2. As shown in Figure 2, the current command u_{RANN} and duty cycle signals d_p are generated by the speed controller and current controller, respectively. The three-phase currents are detected by current sensors and the commutation signals s_p are provided by rotor position sensors. The proposed controller and a PI controller are employed in outer loop and inner loop, respectively.

3. RANN control design

In this section, the RANN controller is designed for SRM drive system with the technique of MLP.

3.1. RBF neural network

In control engineering, RBF NNs are usually used as a tool for approximating the nonlinear function because of their excellent capabilities in function approximation. RBF NNs consist of two layers, which are hidden layer and output layer. The network structure is shown in Figure 3.

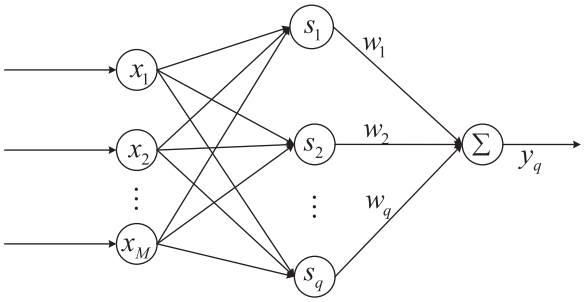

Figure 3. RBF NN structure.

The universal approximation properties show that, if node number q is chosen sufficiently large, then RBF NN can approximate any unknown nonlinear function $f(X)$ to any desired accuracy over the compact set [19]. In this article, we use the following RBF NN to approximate a nonlinear function $f(X)$

$$f(X) = y_q = W^T S(X), \tag{7}$$

where $X = [x_1, x_2, \ldots, x_M]^{\mathrm{T}}$ is the input vector of the RBF NN, y_q is the output of the NN, $W = [w_1, w_2, \ldots, w_q]^{\mathrm{T}}$ is the weight vector of the NN and $S = [s_1(X), s_2(X), \ldots, s_q(X)]^{\mathrm{T}}$ is the basis function that is usually considered Gauss function

$$s_i(X) = \exp\left[-\frac{(X - c_i)^T (X - c_i)}{2\sigma_i^2}\right], \quad i = 1, 2, \ldots, q, \tag{8}$$

where $c_i = [c_{i1}, c_{i2}, \ldots, c_{iM}]^{\mathrm{T}}$ is the centre vector fo the receptive field, and σ_i is the width of the Gauss function. It has been prove that the RBF NN in (7) can approximate any unknown continuous function $f(X)$ over the compact set $\Omega_x \subset R^M$ to arbitrary accuracy as

$$f(X) = W^{*T} S(X) + \varepsilon(X), \quad \forall X \in \Omega_X \subset R^M, \tag{9}$$

where W^* is the optimal weights, $\varepsilon(X)$ is the smallest approximation error. The optimal weight vector W^* is

an "artificial" quantity required only for analytical purposes. Typically, W^* is defined as the value of W that minimizes $|\varepsilon(X)|$ for all $X \in \Omega_X \subset R^M$, i.e.

$$W^* := \arg\min_{W \in R^q} \left\{ \sup_{x \in \Omega_X} |f(X) - W^T S(X)| \right\}. \quad (10)$$

The norm of optimal weight vector W^* of RBF NN and the smallest approximation error $\varepsilon(x)$ are bounded and these can be described as

$$\|W^*\| \leq W_m, \quad |\varepsilon(X)| \leq \varepsilon_m, \quad \forall X \in \Omega_x, \quad (11)$$

where W_m and ε_m are positive constants.

3.2. Design of RANN controller

Define the speed error and its differentiation as follows

$$\begin{aligned} z_1 &= \omega^* - \omega, \\ z_2 &= \dot{\omega}^* - \dot{\omega}, \end{aligned} \quad (12)$$

where ω^* is the desired value of speed. Let the ideal control law be

$$u^*_{\text{RANN}} = \frac{[-A_2\omega + \dot{\omega}^* - d_L + k_1 z_1]}{A_1}, \quad (13)$$

where $k_1 > 0$ is a design parameter.

Substituting (13) into (6), we have

$$[k_1 \quad 1]Z = 0, \quad (14)$$

where $Z = [z_1\ z_2]^{\text{T}}$.

Equation (14) indicates that the motor speed ω can track the speed reference ω^* asymptotically. The ideal control law (13) cannot be carried out because the lamped uncertainty d_L of the system is unknown. According to the equation (9), the RBF NN can be used to approximate the ideal control law (13). Define Z and $\hat{f}(Z) = \hat{W}^T S(Z)$ as the input vector and output variable of the RBF NN, respectively. Using the RBF NN to approximate the ideal control law (13), we have

$$u^*_{\text{RANN}} = W^{*T} S(Z) + \varepsilon, \quad (15)$$

where ε is the minimum approximation error and W^* is the optimum weight vector and can be described as

$$W^* := \arg\min_{W \in R^q} \left\{ \sup_{x \in \Omega_2} |u^*_{\text{RANN}} - W^T S(Z)| \right\}. \quad (16)$$

In order to reduce the number of on-line updating weights of RBF NN, the norm of the optimal weights is considered as an on-line updating parameter [18]. This allows for a n-nodes NN, only one parameter needs to be updated on-line. As a result, the computational burden of the RBF NN-based controller is greatly reduced.

Define the ξ as follows

$$\xi = \|W^*\|^2. \quad (17)$$

To update the weighting vector of RBF NN on-line, the adaptive law of control system can be developed as

$$\dot{\hat{\xi}} = \frac{\gamma}{2a^2} A_1 {z_1}^2 S(Z)^T S(Z), \quad (18)$$

where $\hat{\xi}$ is the estimate of ξ, γ and a are design parameters, $k_0 > 0$ is a small design constant.

Combing (11), (15) and (18), the RANN control is proposed as

$$u_{\text{RANN}} = \frac{1}{2a^2} z_1 \hat{\xi} S(Z)^T S(Z) + \varepsilon_m \operatorname{sgn}(z_1 A_1), \quad (19)$$

where $\operatorname{sgn}(\cdot)$ is sign function that is expressed as

$$\operatorname{sgn}(x) = \begin{cases} 1 & x > 0, \\ 0 & x = 0, \\ -1 & x < 0. \end{cases} \quad (20)$$

In the real applications, a good transient response is desired. However, including the RBF NN, all of the adaptive NN algorithms need some time to approximate the objective function. This means that a large ε_m is needed at the beginning to improve the transient response. But a large ε_m will cause a severe chattering of the control law. In order to improve the transient response and chattering phenomena of the proposed control scheme, a proportional control term is introduced into the proposed control law. Then, the proposed RANN controller is rewritten as

$$u_{\text{RANN}} = \lambda z_1 + \frac{1}{2a^2} z_1 \hat{\xi} S(Z)^T S(Z) + \varepsilon_m \operatorname{sgn}(z_1 A_1), \quad (21)$$

where $\lambda > 0$ is the deign parameter.

4. Stability analysis

Consider the augmented Lyapunov function candidate for the control system consisting of (12), (16), (17) as

$$V(t) = \frac{1}{2} {z_1}^2 + \frac{1}{2\gamma} \tilde{\xi}^2, \quad (22)$$

where $\tilde{\xi} = \xi - \hat{\xi}$.

The time derivative of (22) is

$$\dot{V}(t) = z_1 z_2 - \frac{1}{\gamma} \tilde{\xi} \dot{\hat{\xi}}. \quad (23)$$

From (6), (13) and (19), the following equation can be obtained

$$\begin{aligned} z_2 &= -k_1 z_1 + A_1 (u^*_{\text{RANN}} - u_{\text{RANN}}) \\ &= -(k_1 + \lambda A_1) z_1 + A_1 W^{*T} S(Z) + A_1 \varepsilon \\ &\quad - \frac{A_1 z_1 \hat{\xi} S(Z)^T S(Z)}{2a^2} - A_1 \varepsilon_m \operatorname{sgn}(z_1 A_1). \end{aligned} \quad (24)$$

Substituting (24) into (23), we have

$$\dot{V}(t) = -(k_1 + \lambda A_1){z_1}^2 + A_1 z_1 W^{*T} S(Z) + A_1 z_1 \varepsilon - \frac{A_1 z_1^2 \hat{\xi} S(Z)^T S(Z)}{2a^2} - A_1 z_1 \varepsilon_m sgn(z_1 A_1) - \frac{1}{\gamma}\tilde{\xi}\dot{\hat{\xi}}. \quad (25)$$

According to Young's inequality $ab \le \frac{1}{2}(a^2 + b^2)$, we have

$$z_1 W^{*T} S(Z) \le \frac{z_1^2 \xi S(Z)^T S(Z)}{2a^2} + \frac{a^2}{2}. \quad (26)$$

Substituting (26) into (25) yields

$$\dot{V}(t) \le -(k_1 + \lambda A_1){z_1}^2 + A_1 z_1 \varepsilon + \frac{A_1 z_1^2 \tilde{\xi} S(Z)^T S(Z)}{2a^2} - A_1 z_1 \varepsilon_m \,\mathrm{sgn}(z_1 A_1) - \frac{1}{\gamma}\tilde{\xi}\dot{\hat{\xi}}. \quad (27)$$

Combining (18) with (27), we have

$$\begin{aligned}\dot{V}(t) &\le -(k_1 + \lambda A_1){z_1}^2 + A_1 z_1 \varepsilon + \frac{A_1 z_1^2 \tilde{\xi} S(Z)^T S(Z)}{2a^2} - A_1 z_1 \varepsilon_m sgn(z_1 A_1) - \frac{1}{\gamma}\tilde{\xi}\frac{\gamma}{2a^2} A_1 {z_1}^2 S(Z)^T S(Z) \\ &= -(k_1 + \lambda A_1){z_1}^2 + A_1 z_1 \varepsilon - A_1 z_1 \varepsilon_m \,\mathrm{sgn}(z_1 A_1) \\ &\le -(k_1 + \lambda A_1){z_1}^2 \le 0. \end{aligned} \quad (28)$$

This implies that $\dot{V}(t)$ is a negative semidefinite function. Define the following term:

$$P(t) = (k_1 + \lambda A_1){z_1}^2 \le -\dot{V}(t). \quad (29)$$

Because $V(t)$ is bounded and $V(t)$ is non-increasing and bounded, then

$$\int_0^t P(\tau)\,\mathrm{d}\tau \le V(0) - V(t) < \infty. \quad (30)$$

In addition, because $\dot{P(t)}$ is bounded, it can be shown that $\lim_{t\to\infty} P(t) = 0$ by Barbalat's lemma [20], i.e. $z_1 \to 0$ as $t \to \infty$. Then, the stability of the control system is guaranteed.

5. Simulations

In this section, the simulations are carried in Matlab/Simulink software to evaluate the performance of the proposed RANN controller. Further, the comparative studies are conducted between the proposed RANN controller and conventional PI controller. A three-phase 1.5 kW 12/8 poles SRM is used in the simulation and experimental investigation in this paper. Detailed parameters of the SRM are presented in Table 1. The simulation model of the 12/8 poles SRM is obtained by taking the off-line measurement of electromagnetic characteristics of this motor. The measured flux-linkage and static torque characteristics are described in Figure 4.

Table 1. Specifications of SRM.

Parameter	Value
Phase	3
Stator poles	12
Rotor poles	8
Rated power	1.5 kW
Rated torque	9.55 N m
Speed range of constant torque	100–1500 r/min
Maximum flux linkage	0.986 Wb
Stator resistance	0.9 Ω
Moment of inertia J	0.01 kg m^2
Friction coefficient k_ω	0.005 N m s

The design parameters of proposed RANN controller are chosen as: $\lambda = 0.02$, $a = 13$, $\gamma = 1$, $\varepsilon_m = 0.1$, $A_1 = 25$, $A_2 = -0.5$ and $A_3 = -100$. The design parameters of the RBF NN are selected as: node number $q = 10$, the centres $c_i (i = 1, 2 \ldots 10)$ evenly spaced in $[-100, 100] \times [-100, 100]$, and the width $\sigma_i = 50 (i = 1, 2 \ldots 10)$. The parameters ($K_{pc}$ and K_{ic}) of current PI controller are obtained by trial-and-error method to achieve satisfactory current tracking effect. The tuned parameters of inner-loop current controller are $K_{pc} = 0.3$ and $K_{ic} = 0.1$. The satisfactory performance parameters $K_p = 0.1$ and $K_i = 0.4$ of the conventional PI controller were obtained through fine tuning at a motor rated speed. Note that all of the reference speeds in simulations are set for with 1500 r/min/s slope.

Firstly, three different combinations for λ and ε_m are set up to verify the beneficial effects of introducing proportional control term. Secondly, the comparisons between the proposed RANN controller and conventional PI controller are conducted at different speed references (100 r/min and 1500 r/min) with external load $T_L = 1$ Nm to test their wide range speed response capability. Thirdly, two parameter variations that the friction coefficient k_ω: 0.01 → 0.02 and the moment of inertia J: 0.005 → 0.01 are exerted to evaluate the robustness of proposed controller. Finally, an external step load T_L which is changed from 1 Nm to 9.55 Nm is applied at steady state to verify the anti-disturbance performance of the proposed controller. The speed response ω, speed error z_1, phase flux linkage ψ_p, phase currents i_p and control effort u_{RANN} are shown in each subplot.

With $\lambda = 0$ and $\varepsilon_m = 0.1$, Figure 5(a) shows that the maximum transient speed error is approximately 79 r/min. Small ε_m lead to a large speed error. In Figure 5(b), the maximum speed error is obviously lower because large ε_m caused a compensation. However, the larger ε_m also caused undesired chattering of the control input u. Therefore, it is difficult to achieve satisfactory results without introducing proportional term. Figure 5(c) presents the simulation

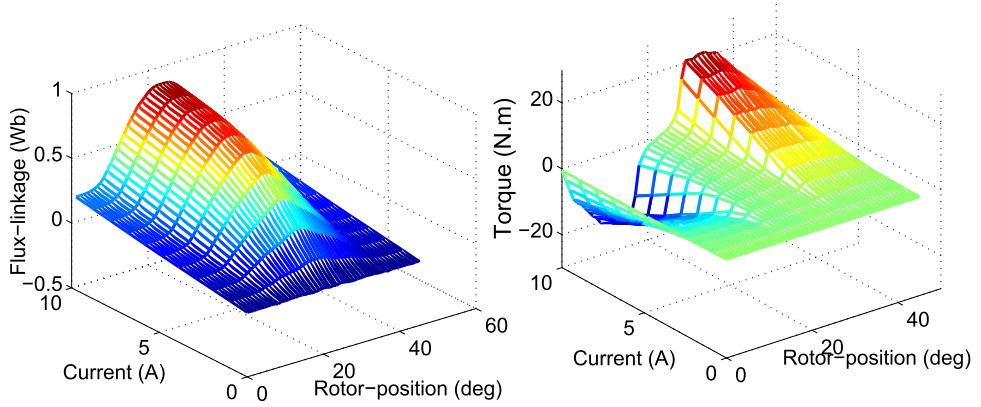

Figure 4. Measured electromagnetic characteristics of the SRM.

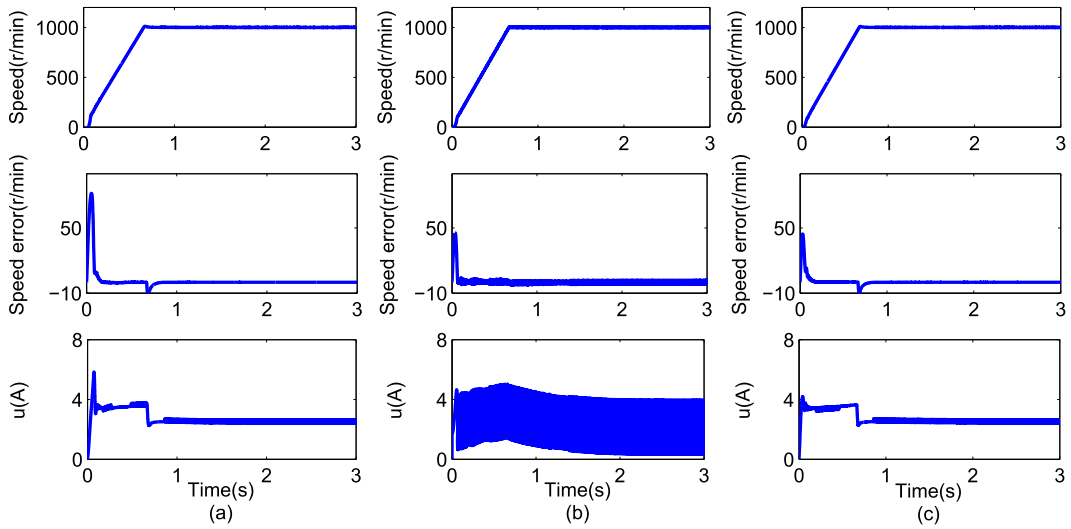

Figure 5. Simulation results of the RANN controller for the SRM drive. (a) $\lambda = 0$ and $\varepsilon_m = 0.1$. (b) $\lambda = 0$ and $\varepsilon_m = 1.8$. (c) $\lambda = 0.02$ and $\varepsilon_m = 0.1$.

results of the proposed RANN control with $\lambda = 0.02$ and $\varepsilon_m = 0.1$. It can be seen that the RANN controller after introducing proportional term not only has small transient speed error but also effectively reduces chattering. Figure 6(a,b) depict the simulation results of the proposed controller and conventional PI controller at speed command 1500 r/min. In Figure 6, the maximum speed error of the proposed controller and PI controller are 41.01 and 45.55,r/min, respectively. And the steady-state speed error of the proposed controller and conventional PI controller are 0.4 and 0.7 r/min, respectively. The simulation results of the proposed controller and conventional PI controller at speed command 100 r/min is shown in Figure 7(a,b). In Figure 7, the maximum speed error of the proposed controller and conventional PI controller are 40.09 and 45.57 r/min, respectively. The steady-state speed error of the proposed controller and conventional PI controller are 1.13 and 1.22 r/min, respectively. From Figures 6 and 7, in addition, we can see that the settling time of the proposed controller is much less than that of the conventional PI controller. The results indicate that the proposed RANN controller has better speed tracking capability compared with the conventional PI control over a wide speed range.

Figure 8(a,b) plot the simulation results of the proposed RANN controller and conventional PI controller under parameter variations in J and k_ω, respectively. As shown in Figure 8(a), the maximum speed error and the steady speed error of the proposed controller are 44.52 and 0.27 r/min, respectively. Figure 8(b) presents the simulation results of the conventional PI controller, where the maximum speed error and the steady speed error are 51.68 and 0.65 r/min, respectively. Figure 8 indicates that the proposed controller can track the speed reference vary well in the presence parameter variations. That is because that the proposed RANN controller has a good adaptive capability for parameter variations.

Figure 9(a,b) present the simulation results obtained using the proposed controller and conventional PI controller at 1500 r/min command speed with a step external load $T_L = 1\,\text{Nm} \rightarrow 9.55\,\text{Nm}$ applied in 1.5 s. Figure 9(a) shows the simulation results of proposed controller, where the maximum speed dip is 50.92 r/min, and the speed error backs to the range

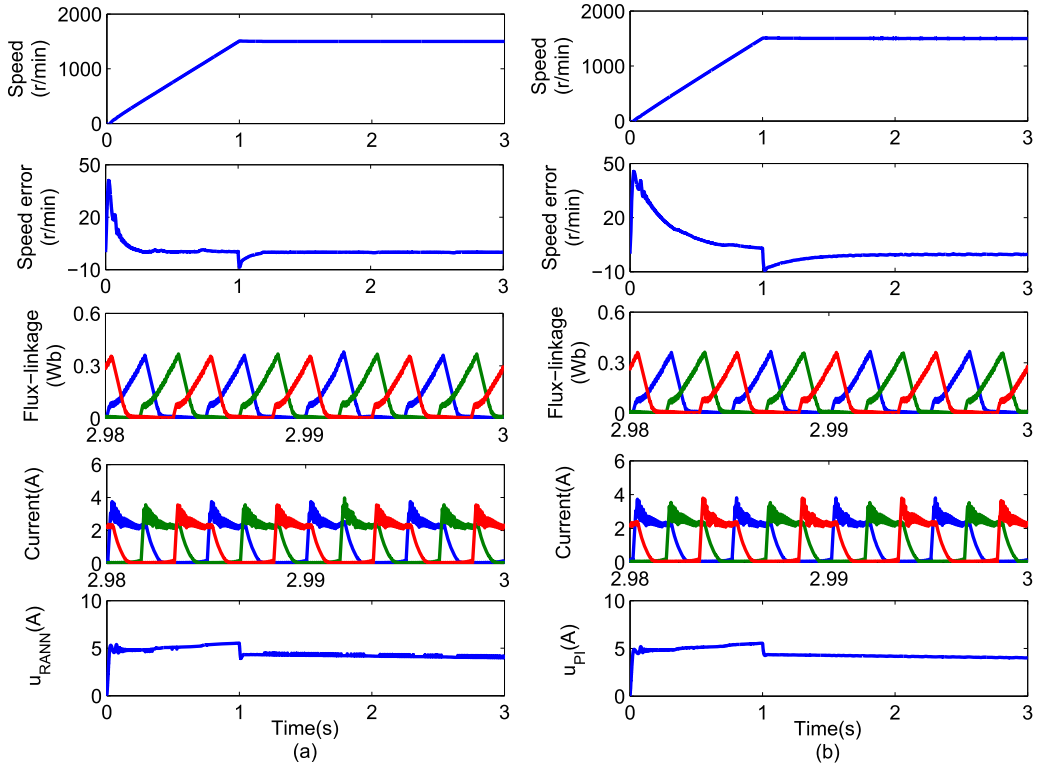

Figure 6. Simulation results at 1500 r/min speed reference with external load T_L =1 Nm. (a) RANN controller and (b) PI controller.

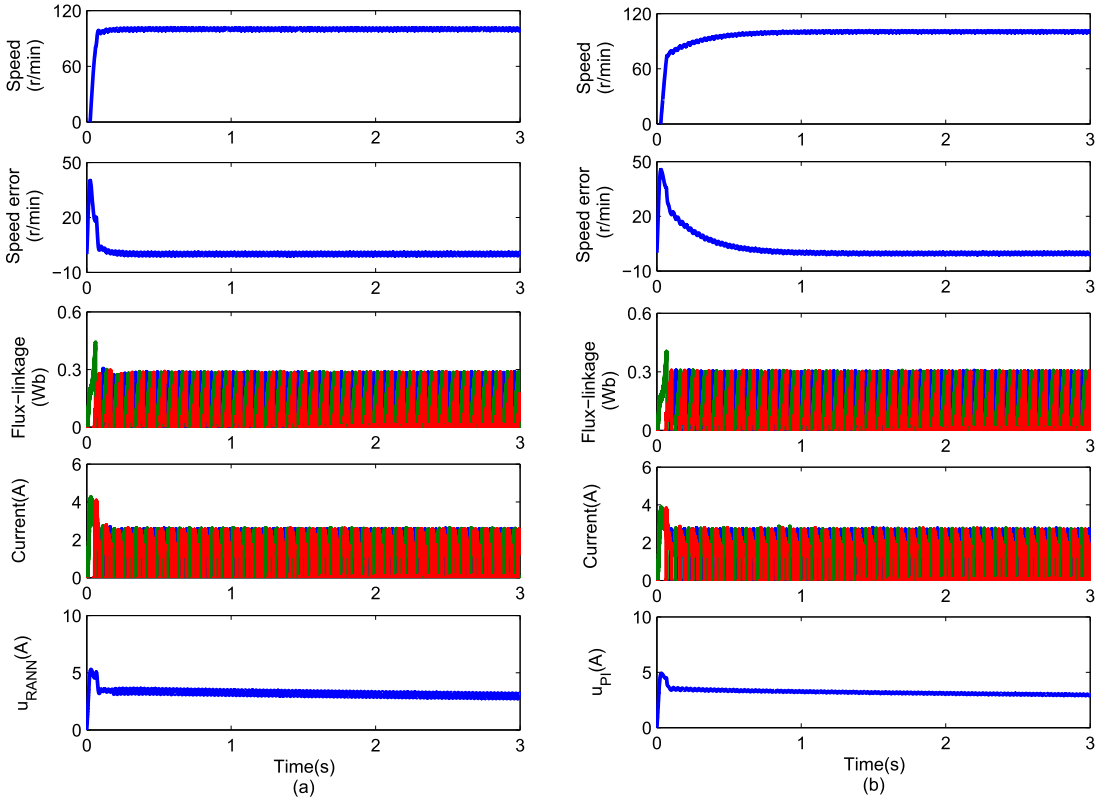

Figure 7. Simulation results at 100 r/min speed reference with external load T_L =1 Nm. (a) RANN controller and (b) PI controller.

of 0.5 r/min only through 0.3 s. Figure 9(b) presents the simulation results of the conventional PI controller under the same conditions, where the maximum speed dip is 51.34 r/min, and the speed error recovers to the range of 0.5 r/min through 1.0 s. The results indicate that the proposed controller has the better robustness against the external load disturbance than the conventional PI controller.

In general, the proposed control scheme has a excellent speed regulation performance, especially when the parameters and external load change, still can maintain high performance speed control. Hence, the

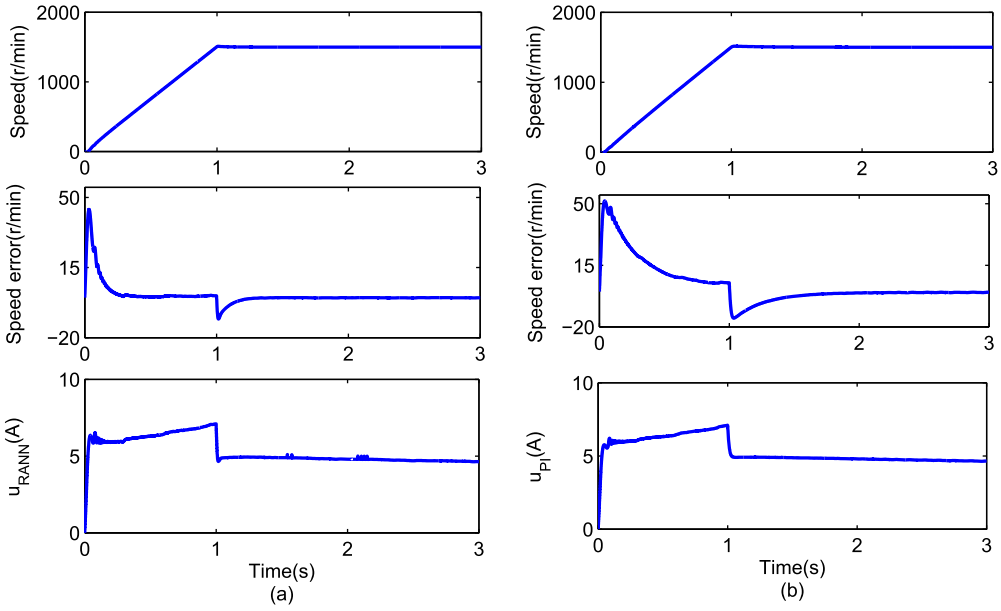

Figure 8. Simulation results at 1500 r/min speed reference with 100% parameter variations: $J = 0.01 \rightarrow 0.02$ and $k_\omega = 0.005 \rightarrow 0.01$. (a) RANN controller and (b) PI controller.

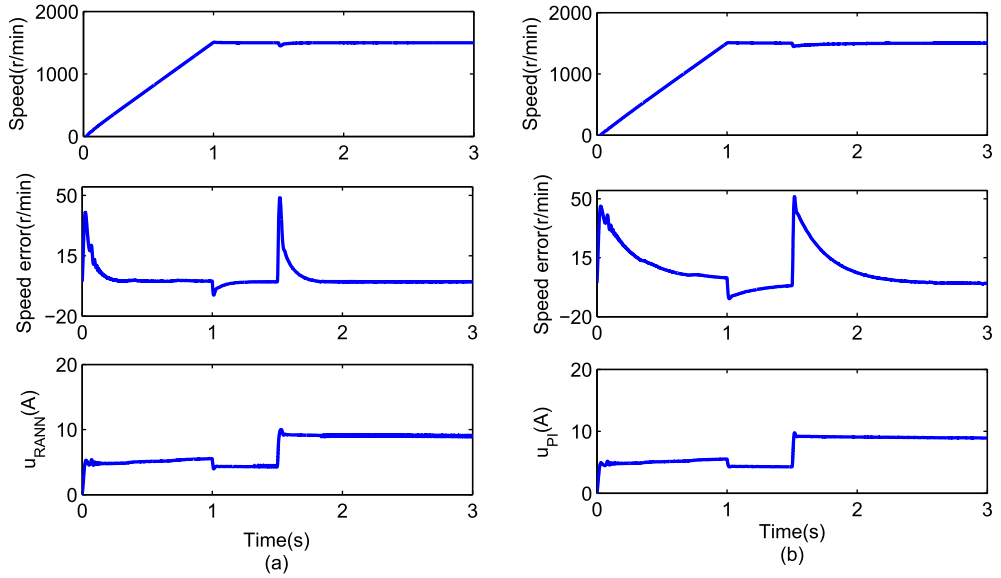

Figure 9. Simulation results at 1500 r/min speed reference with an external step load disturbance T_L =1 Nm $\rightarrow$ 9.55 Nm applied at 1.5 s. (a) RANN controller and (b) PI controller.

effectiveness of the proposed RANN controller is verified by simulation. The proposed control scheme will be implemented on a practical SRM to demonstrate its practicality in the following section.

6. Experiments

In this section, the experimental results are presented with a three-phase 12/8 poles 1.5 kW SRM. Detail motor parameters are listed in Table 1. The SRM test bench is shown in Figure 10. A magnetic particle brake acts as a load on the SRM test system. The desired load torque can be obtained by regulating the excited current of magnetic particle brake. Control algorithm and data logging are programmed in DS1103 which produced by dSPACE company. The SRM is driven by an asymmetrical half-bridge dc-dc converter, which consists of six IGBT gates. Hall-effect sensors are used for current and voltage measurements, respectively. The sampling frequencies in the experimental study are set to be 1 and 10 kHz for outer loop (speed control) and inner loop (current control), respectively. The experimental data were gathered and processed by computer. All of the reference speeds in experiments are set for with 1000 r/min/s slope.

The investigations were performed as follows to demonstrate the wide range speed tracking capability and the robustness against the external load disturbance of the proposed RANN controller. Firstly, the proposed RANN controller is operated at two speed

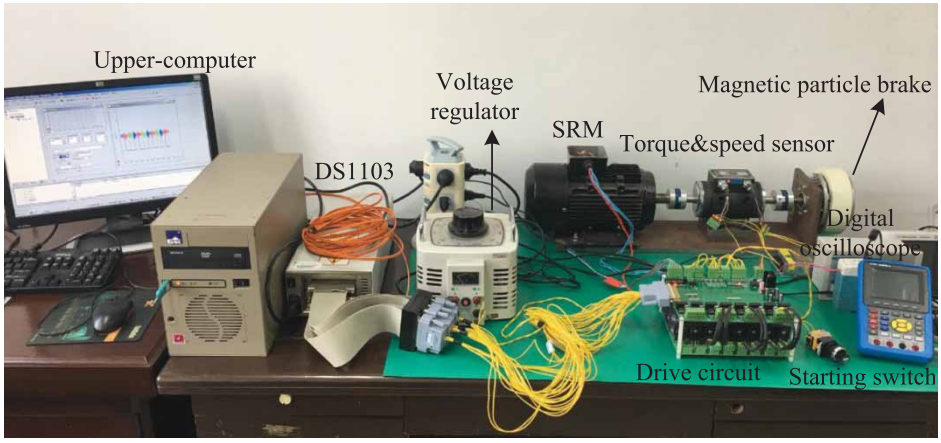

Figure 10. Experimental bench.

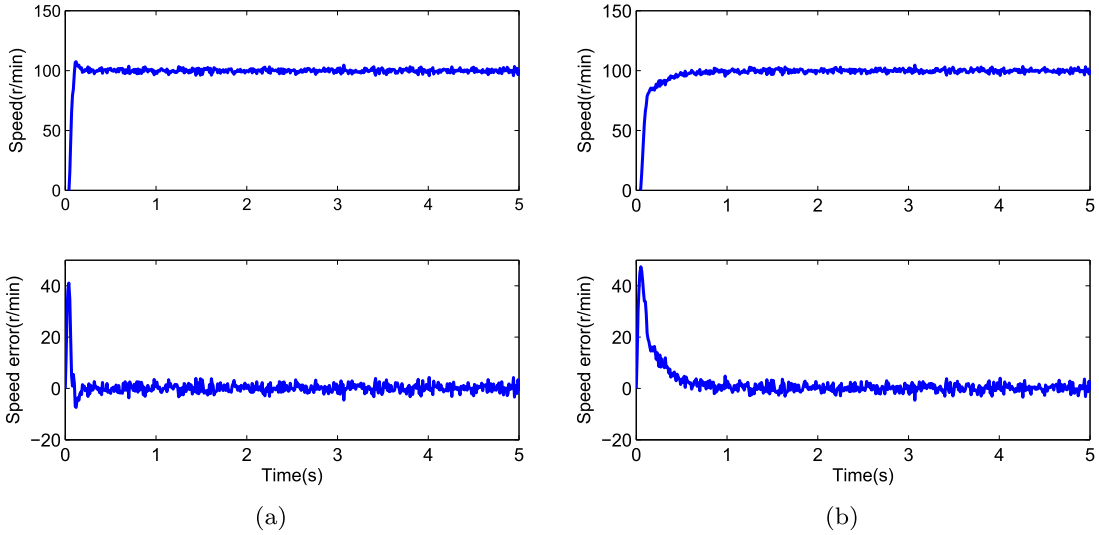

Figure 11. Experimental results at 100 r/min speed reference with external load $T_L = 1$ Nm. (a) RANN control and (b) PI control.

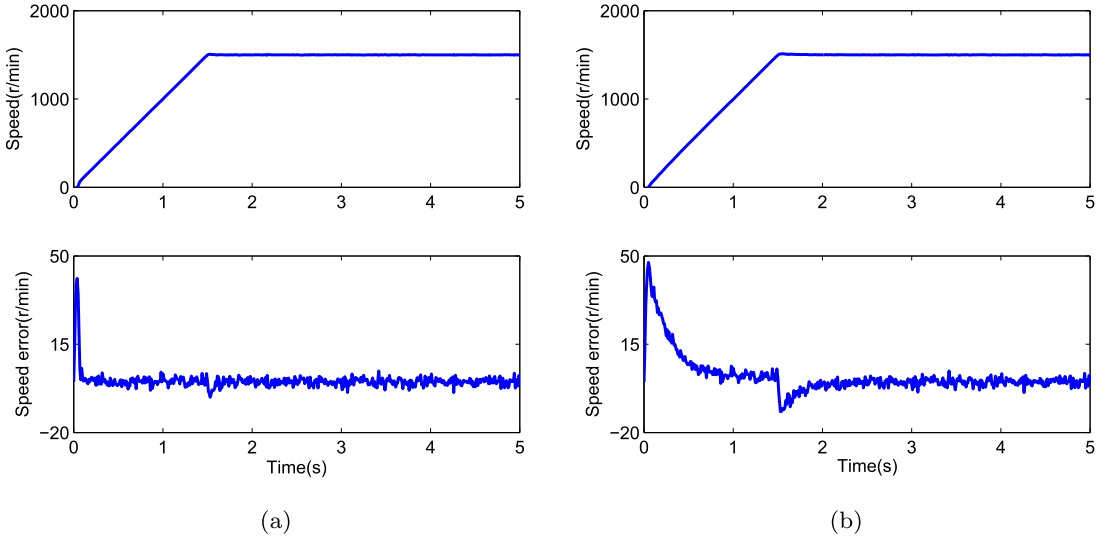

Figure 12. Experimental results at 1500 r/min speed reference with external load $T_L = 1$ Nm. (a) RANN control and (b) PI control.

references (100 and 1500 r/min) to confirm the full range speed tracking capability. Secondly, for testing the robustness, the proposed controller is started with load $T_L = 1$ Nm, and an external load $T_L = 5$ Nm is applied at 2.5 s when the system operated in steady state. In the experimental studies, the conventional PI control is also carried out in the same condition to compare their speed performance with proposed RANN controller.

Figures 11 and 12 present that the experimental results obtained at 100 and 1500 r/min reference speeds

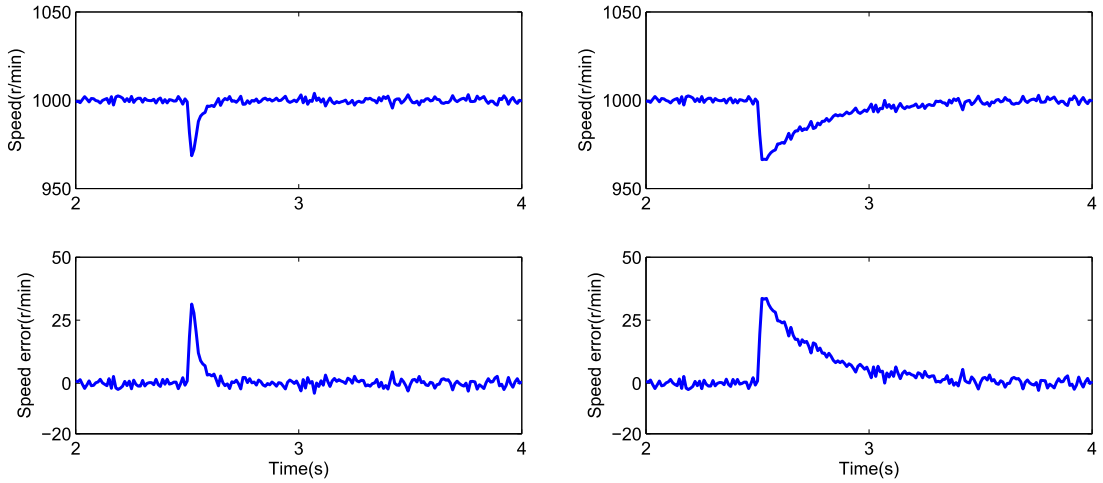

Figure 13. Experimental results at 1000 r/min speed reference with an external step load disturbance $T_L = 1\,\text{Nm} \rightarrow 5\,\text{Nm}$ applied at 2.5 s. (a) RANN control and (b) PI control.

Table 2. Comparison of RMSE.

Speed reference	RANN controller	PI controller
100 r/min	3.7912	6.4715
1500 r/min	3.8194	7.8396
1000 r/min	4.4230	8.8477

with 1 Nm external load. The speed response ω and speed error z_1 are shown in each subplot. Figure 13 shows that the experimental results for the control system with external step load $T_L = 1\,\text{Nm} \rightarrow 9.55\,\text{Nm}$ applied at 2.5 s in the steady state. The speed response ω and the speed error z_1 of the proposed controller and conventional PI controller are shown in Figure 13(a,b), respectively. In order to quantitatively evaluate the control performance of the proposed RANN controller and PI controller, the experimental RMSEs are summarized in Table 2. The performance index, RMSE, is defined as follows:

$$J_{\text{RMSE}} = \sqrt{\frac{1}{N}\sum_{n=1}^{N} z_1^2(n)}, \tag{31}$$

where N is the number of the sampled points.

Table 2 clearly indicates that the RANN controller is superior than the conventional PI control under different operational speeds. Moreover, it is observed from Figure 13, that the speed dips of the proposed controller and conventional PI controller are all approximately 38 r/min. But the measured speed of proposed controller recovers the speed reference (1000 r/min) more quickly than conventional PI controller. This experimental results indicated that the proposed controller has a good robustness to against the external disturbance.

In summary, the performances of conventional PI control are unsatisfactorily in a wide range of speeds, parameter variations, especially in the case of external load disturbances. In contrast, the proposed RANN controller exhibits the similar satisfactory control performance in each case.

This is because that the conventional PI control with fixed parameters is weak in resisting external disturbance and has not the adaptability to parameter variations, whereas the proposed RANN controller has the adaptability and the better robustness due to exploiting the universal approximation ability and the on-line learning ability of adaptive NN. In the proposed control scheme, the parameter variations and external load disturbances of the SRM drive system can be compensated by the adaptive RBF NN.

7. Conclusions

In this article, a robust adaptive RBF NN control scheme has been developed for SRM drive system with parameter variations and external load disturbances. The desirable control law including parameter variations and external load disturbances is approximated by using an RBF NN. The proposed controller is derived in the sense of Lyapunov function, and thus, the control system can be guaranteed to be semi-global asymptotic stability. The adaptive law of the proposed controller is derived by combining MLP technique, which makes only one parameter that needs to be updated on-line for n-nodes NN. As a result, the proposed controller is very easy to be implemented in digital processor. The comparative studies are carried out by simulations and experiments to confirm the control performance of the proposed controller. The simulation and experimental results demonstrate that the proposed controller has superior adaptive ability for parameter variations and robustness to against external disturbance. In the future research, we will consider the four quadrant speed control and improve the efficiency of SRM drive system.

Disclosure statement

No potential conflict of interest was reported by the authors.

Funding

This work was supported by National Natural Science Foundation of China [grant number 51407021].

ORCID

Cunhe Li http://orcid.org/0000-0001-8379-1861

References

[1] Vijayakumar K, Karthikeyan R, Paramasivam S, et al. Switched reluctance motor modeling, design, simulation, and analysis: a comprehensive review. IEEE Trans Magn. 2008;44(12):4065–4617.
[2] Boldea I, Tutelea LN, Parsa L, et al. Automotive electric propulsion systems with reduced or no permanent magnets: an overview. IEEE Transn Ind Electron. 2014;61(10):5696–5711.
[3] Sozer Y, Husain I, Torrey DA. Guidance in selecting advanced control techniques for switched reluctance machine drives in emerging applications. IEEE Trans Ind Appl. 2015;51(6):4505–4514.
[4] Wang XL, Xu ZL. Speed regulation control of switched reluctance motors based on PI parameters self-adaptation. Proc CSEE. 2015;35(16):4215–4223.
[5] Spong MI, Marino R, Peresada SM, et al. Feedback linearizing control of switched reluctance motors. IEEE Trans Automat Control. 1987;32(5):371–379.
[6] Shang WF, Ma HW, Wang CW. Internal model control of switched reluctance motor with torque observer for plant-model mismatches. Proc Inst Mech Eng I J Syst Control Eng. 2013;227(4):403–412.
[7] Chen C, Liu T. Nonlinear controller design for switched reluctance drive systems. IEEE Trans Aerosp Electron Syst. 2003;39(4):1429–1440.
[8] Buja GS, Menis R, Valla MI. Variable structure control of an SRM drive. IEEE Trans Ind Electron. 1993;40(1):56–63.
[9] Zhong R, Xu YZ, Cao YP, et al. Accurate model of switched reluctance motor based on indirect measurement method and least square support vector machine. IET Electric Power Appl. 2016;10(9):916–922.
[10] Song SJ, Ge LF, Zhang M. Data-reconstruction-based modeling of SRM with few flux-linkage samples from torque-balanced measurement. IEEE Trans Energy Convers. 2016;31(2):424–435.
[11] Lu WZ, Keyhani A, Fardoun A. Neural network-based modeling and parameter identification of switched reluctance motors. IEEE Trans Energy Convers. 2003;18(2):284–290.
[12] Li CH, Wang GF, Fan YS, et al. A self-tuning fuzzy PID speed control strategy for switched reluctance motor. Proceedings of the 28th CCDC; 2016. p. 3084–3089.
[13] Zheng JM, Zhao SD, Wei SG. Application of self-tuning fuzzy PID controller for a SRM direct drive volume control hydraulic press. Control Eng Pract. 2009;17:1398–1404.
[14] Wei SG, Zhao SD, Zheng JM, et al. Self-tuning dead-zone compensation fuzzy logic controller for a switched-reluctance-motor direct-drive hydraulic press. Proc Inst Mech Eng I J Syst Control Eng. 2009;223:647–656.
[15] Tseng CL, Wang SY, Chien SC, et al. Development of a self-tuning TSK fuzzy speed control strategy for switched reluctance motor. IEEE Trans Power Electron. 2012;27(4):2141–2152.
[16] Wang SY, Tseng CL, Chien SC. Adaptive fuzzy cerebellar model articulation control for switched reluctance motor drive. IET Electric Power Appl. 2012;6(3):190–202.
[17] Yang YS, Feng G, Ren JS. A combined backstepping and small-gain approach to robust adaptive fuzzy control for strict-feedback nonlinear systems. IEEE Trans Syst Man Cybern A Syst Humans. 2004;34(3):406–420.
[18] Chen B, Liu XP, Liu KF, et al. Direct adaptive fuzzy control of nonlinear strict-feedback systems. Automatica. 2009;45:1530–1535.
[19] Sanner RM, Slotine JE. Gaussian networks for direct adaptive control. IEEE Trans Neural Netw. 1992;3:837–863.
[20] Slotine JJE, Li W. Applied nonlinear control. Englewood Cliffs (NY); Prentice-Hall; 1991.